

Reflective liquid crystal polarization gratings with high efficiency and small pitch

Ravi K. Komanduri, Chulwoo Oh, and Michael J. Escuti

North Carolina State Univ, Dept Electrical & Computer Engineering, Raleigh, NC (USA)

ABSTRACT

We report our experimental success in realizing high efficiency liquid crystal polarization gratings (LCPGs) on reflective substrates, with periods as small as $2.2\mu\text{m}$, enabling the largest switchable LCPG diffraction angles reported yet for red light. Moreover, these gratings retain nearly ideal electro-optical properties, including $> 95\%$ hologram efficiency, high polarization contrast, sub-millisecond total switching times, and relatively low voltage operation (thresholds $\sim 1.5\text{V}$). We discuss two different fabrication approaches, each with its own set of advantages, which have resulted in gratings with the above compelling properties. We anticipate broad utility of these diffractive elements in a variety of applications.

Keywords: reflective, polarization gratings, liquid crystal

1. INTRODUCTION

Liquid Crystal Polarization Gratings (LCPGs)¹⁻⁴ have been identified as switchable diffractive elements that are capable of modulating light with nearly 100% efficiency. These fall under the general category of electrically tunable diffraction gratings and impact a broad spectrum of applications, including but not limited to optical-filters, displays, polarimetry, beam-steering, remote-sensing, etc. In this paper, we discuss the compelling characteristics of reflective LCPGs and two fabrication methods that have resulted in high-quality gratings with grating periods as low as $2.2\mu\text{m}$. Both of these methods are generally applicable to the broader category of continuous LC gratings and extend the holographic fabrication process to any type of reflective substrate. Here we investigate some of the electro-optical properties of reflective LCPGs and report on some of our experimental work that improves upon our previous results with transmissive substrates. These properties are suitable for making highly efficient, compact, and low power consuming tunable optical devices.

2. BACKGROUND

Most commercial LC devices suffer from the use of polarizers that limit their maximum achievable efficiency to less than 50%. Reflective Spatial Light Modulators (SLMs) based on Liquid Crystal On Silicon (LCOS) technology have the advantages over the transmissive-mode of higher resolution and fill-factors, due to the mature microelectronics industry. But all conventional LC devices (reflective and transmissive) also suffer from the same losses because of polarizers. Therefore, the efficiency of practically all commercially relevant LC devices could be roughly doubled, if a polarizer-free LC technology could be developed. To tackle this problem, a variety of different solutions, many of which involve the use of diffraction gratings,^{2,5-9} have been suggested.

In the context of reflective LC gratings for polarization independent modulation, only a few of these approaches stand out. Among these methods, one popular scheme is to create volume-Bragg gratings using polymer dispersed liquid crystals.^{5,8,10} Holographically patterned Polymer Dispersed Liquid Crystals, also known as H-PDLCs consist of periodically arranged layered dispersions of LCs and polymers resulting in Bragg-diffraction that can be controlled electrically.^{5,8,10} Absolute diffraction efficiencies as high as 80 – 90% have been reported using H-PDLCs.¹⁰ But the maximum efficiency reported in literature is limited by scattering, attributed to the complex fabrication process, and generally high driving voltages in the order of 100 V are required to modulate their optical properties.

Correspondence should be sent to: mjescuti@ncsu.edu, Telephone: +1 919 513 7363

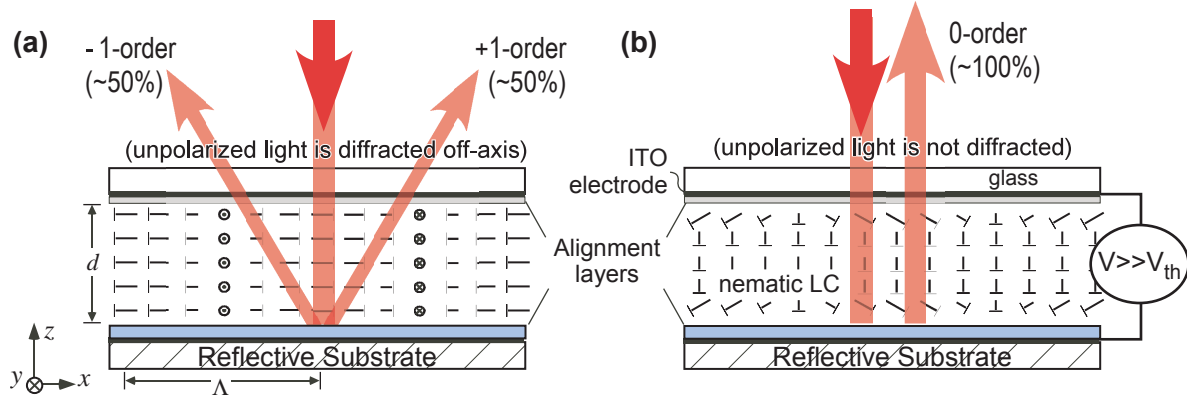


Figure 1. Cross-sectional view of the reflective LCPG in the (a) OFF and (b) ON states. In the OFF state, the incident unpolarized light is diffracted off-axis, but when the voltage is applied in ON state, most of this light is reflected back.

The second major category is comprised of nematic LC diffraction gratings. Among these, nematic LC Polarization Gratings^{1-4, 11} (LCPGs) have emerged as the most promising candidates. PGs in general are periodic anisotropic structures that modulate the polarization state of incident light unlike conventional amplitude and phase gratings. Several different types of liquid crystal PGs,^{6, 7, 9} that can also theoretically modulate light with 100% efficiency, have been studied. Some of these PGs^{7, 9} have been implemented on reflective substrates, but less than ideal results have been obtained experimentally. The discrete nature of most of these, coupled with the fabrication processes such as micro-rubbing,⁹ has resulted in the less than ideal experimental results. In our previous work,^{3, 4} we have considered one particular class of PGs, with the spiraling texture shown in Fig. 1(a), and have demonstrated their viability for a variety of applications, by achieving experimental diffraction efficiencies of $> 99\%$ on transmissive substrates. This structure can be fabricated by holographically patterning the alignment layers shown in the figure. Transmissive, defect-free, LCPGs have therefore been developed through a combination of factors, such as the choice of photo-alignment materials with high enough anchoring strength,¹² thin-film processing parameters, and a better understanding of the relations between material properties and LCPG device parameters.¹³

Holographic fabrication of LCPGs cannot be easily applied to reflective substrates due to interference from the back-reflection, which is especially a problem with SLMs that have patterned surfaces. Therefore, in order to take advantage of the optical properties of LCPGs, the traditional fabrication process has to be revised. Here we report on two such alternatives that allow us to make reflective LCPGs which can diffract light with $> 95\%$ efficiency. In addition, we will take a look at some other advantages that reflective LCPGs offer over the transmissive mode, such as allowing for fabrication at smaller grating periods, faster electrical dynamic response, etc. These impressive properties point toward highly-efficient LCOS SLMs and any other application that could benefit by a reflective modulator that is polarization-independent.

3. REFLECTIVE POLARIZATION GRATINGS

Here we revisit some of the basic optical properties of reflective LCPGs. The continuously rotating pattern in Fig. 1(a) can be represented by the nematic director defined by $\mathbf{n}(x) = \cos(\pi x/\Lambda)\mathbf{x} + \sin(\pi x/\Lambda)\mathbf{y}$. The unique properties of this structure is that it splits the incident light into just three diffraction orders. For the reflective LCPG shown, under normal incidence and assuming an ideal mirror, the traditional expressions for the transmissive case³ can be extended to the reflective mode which leads to the following:

$$\eta_0 = \cos^2\left(\frac{2\pi\Delta nd}{\lambda}\right), \quad (1)$$

$$\eta_{\pm 1} = \frac{1 \pm S'_3}{2} \sin^2\left(\frac{2\pi\Delta nd}{\lambda}\right). \quad (2)$$

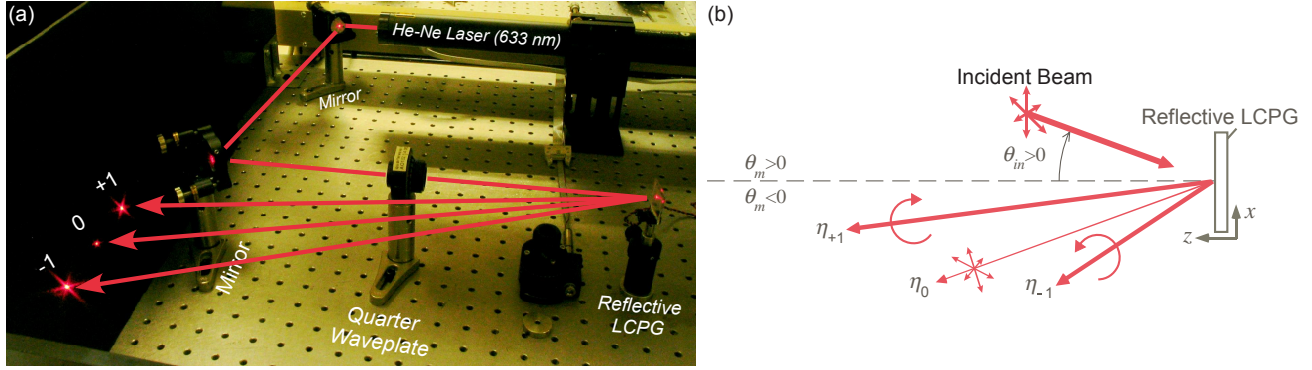


Figure 2. (a) Snapshot image showing the three diffracted orders from a reflective LCPG. (b) Schematic representation showing the notation for the angles and polarization states of the incident and diffracted beams.

Here d is the grating thickness, Δn is the birefringence of the LC material, λ is the wavelength, and $S'_3 = S_3/S_0$ is the normalized Stokes' parameter.¹⁴ When $d = \lambda/(4\Delta n)$, these expressions predict that under no applied field, the LCPG should split the incident light into just the two first orders, as shown in Fig. 1(a). When a voltage much larger than the threshold voltage is applied, the LC molecules realign along the applied field, erasing the grating pattern, which causes the incident light to redirect into the 0-order as shown in Fig. 1(b).

In Fig. 2(a), an image of the actual diffraction from a reflective LCPG, with no voltage applied, designed based on these principles is shown. The light source is a linearly polarized He-Ne laser ($\lambda = 633 \text{ nm}$), whose polarization state is controlled by the Quarter Waveplate (QWP). Light from the QWP is incident on the reflective LCPG sample at an incident angle $\approx 5^\circ$, which diffracts this incident light into just three diffracted orders, the notation for which is shown in Fig. 2(b). It can be easily seen that most of the diffracted light appears in the ± 1 orders and the leakage in the 0-order is small. In the specific example of Fig. 2(a), the fast-axis of the QWP is parallel to the polarization of the laser source and hence the incident light is vertically polarized. So in Eq. (2), this corresponds to $S'_3 = 0$ which translates into nearly equal diffracted power in the ± 1 orders, which can also be roughly verified from the image.

We have earlier pointed out that an additional design constraint has to be imposed, which is represented by¹³

$$d_C = \frac{\Lambda}{\sqrt{0.6 + 0.4 \left(2 \frac{K_3}{K_1} - \frac{K_2}{K_1} \right)}}, \quad (3)$$

assuming strong alignment condition at the surface. Here d_C is the critical thickness for the LCPG, which imposes an upper bound for d to maintain the in-plane orientation shown in Fig. 1(a), derived using elastic continuum principles.¹³ This can also be interpreted to mean that the minimum achievable grating period scales linearly with the cell-gap d . Since reflective LCPGs require half the cell-gap as the transmissive case, for the same LC material, the smallest achievable grating period also decreases by half. Moreover the dynamic response times of LCPGs¹³ are proportional to d^2 and so, reflective LCPGs should have nearly four times faster response times than transmissive samples. Based on these principles, we have fabricated reflective LCPGs with $\Lambda < 2.2 \mu\text{m}$ and with switching times as low as $600 \mu\text{s}$, which will be discussed in the next few sections.

4. HOLOGRAPHIC FABRICATION ON REFLECTIVE SUBSTRATES

In our comparison of reflective LC gratings, we briefly mentioned that holographic interference on reflective surfaces is problematic because of interference from back-reflection. Both recording beams in the polarization hologram reflect off of the surface, which ultimately leads to a complex four-beam interference pattern with large intensity variations. When this complex intensity and polarization pattern is used for recording the grating directly (as we have done in previous unpublished work), it leads to very poor LC alignment, and hence, low efficiencies and high scattering. Ordinarily with transmissive substrates, all alignment layers shown in Fig. 1(a)

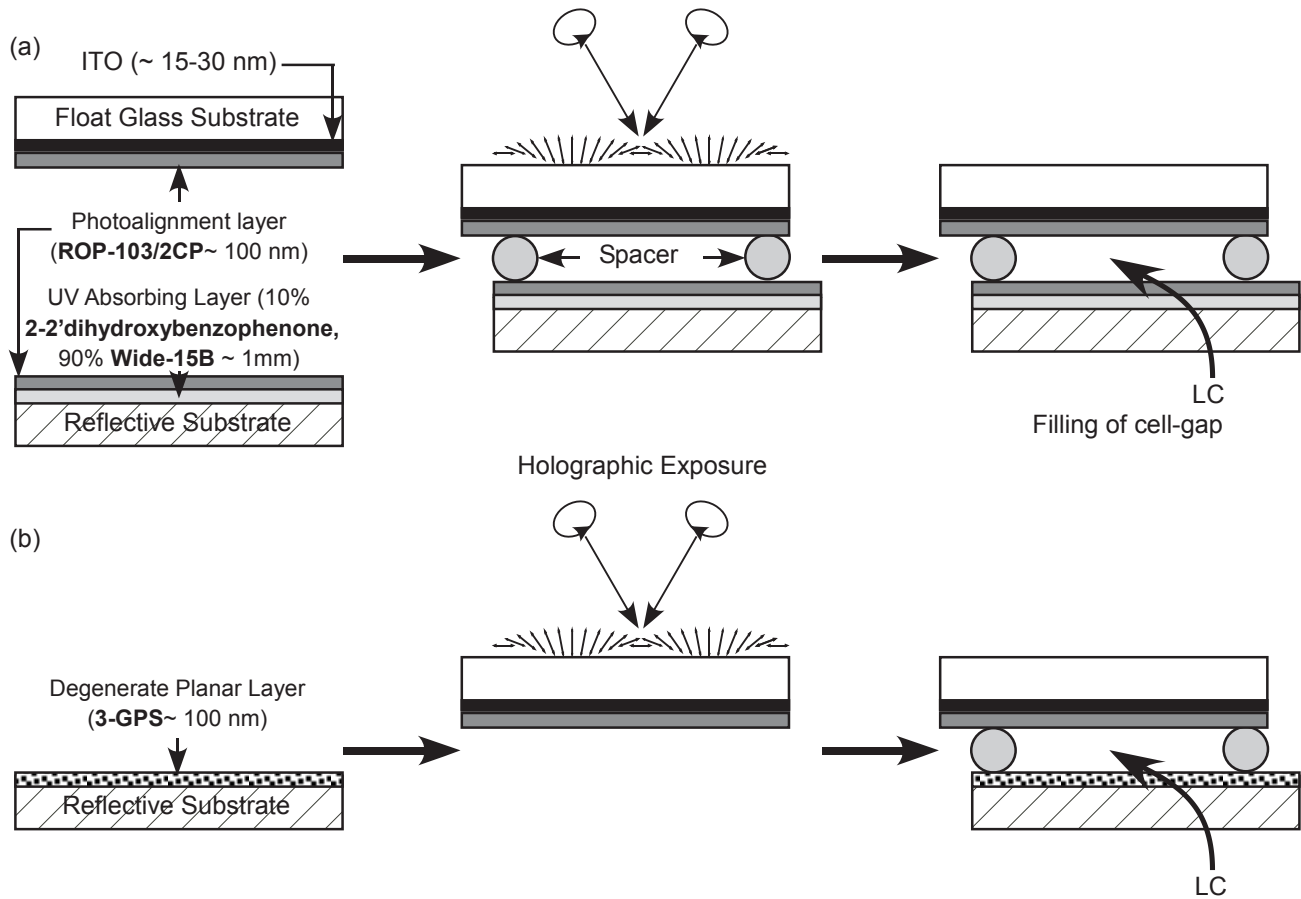


Figure 3. Overview of the reflective LCPG fabrication process listing the important steps with (a) UV absorbing layer and, (b) Degenerate Planar Anchoring approaches respectively.

are layers of photo-alignment materials^{3,4} that are exposed to a holographic interference pattern. Here we discuss two alternative methods to pattern the alignment layers on the reflective substrate to provide essentially the same anchoring condition as before, but which do not suffer from the four-beam interference problem.

4.1. UV Absorbing Thin Film

The first approach is shown in Fig. 3(a). Here the reflective surface is first coated with a thin film of highly absorbing UV film. The basic idea is to use this film and absorb most of the incident light as the hologram is recorded. By trying out different materials and processing conditions, we have come up with the following recipe for making this film: A solution made up of 90 % (wt/wt) of *WiDETM-15B* (commercially available from Brewer Sci. Ltd.) and 10% (wt/wt) of 2-2'-dihydroxybenzophenone,¹⁵ is spin coated onto the reflective substrate at 6000 RPM for 1 minute, and then dried at 130°C for 5 minutes. This processing produces ~1 μ m thick films, which was measured using a profilometer. We have also measured the reflectance of an aluminum mirror (MF31-419, Edmund Optics Ltd.) coated with these films. The reflectance at 325 nm (the recording wavelength in our process) of this 1 μ m layer is only about 10%. But when a spectrum is measured for the same sample over the entire visible range from 450 – 750nm, the reflectance is nearly identical to the bare mirror reflectance. Therefore, the UV absorbing film is essentially transparent over the entire visible range.

Once this layer is coated, the rest of the processing is the same as the transmissive case and is shown in Fig. 3(a). On both the ITO substrate, and the reflective substrate that is pre-coated with the UV absorbing film, the photo-alignment layer, ROP-103/2CP (Rolic Ltd., Switzerland) is spun at 3000 RPM for 45 s and cured

at 130°C for 5 minutes. Then a sandwich is made with the appropriate cell-gap using a spacer-glue mixture, and exposed to the interference pattern of two orthogonally circularly polarized UV laser beams, as shown. Finally the cell is filled with the LC material in isotropic state at 130°C for 5 minutes. Note that the alignment condition here is exactly the same quality as that on transmissive substrates. The only change is the addition of a thin anti-reflection film coated to preserve the recording process.

4.2. Degenerate Planar Anchoring

The second fabrication approach is shown in Fig. 3(b). In this case, the reflective substrate is not exposed to the interference pattern. Instead it is coated with a thin-layer of 3-GPS¹⁶ ((3-Glycidyoxypropyl)trimethoxysilane, Sigma Aldrich Ltd.), a material that provides degenerate planar anchoring and tries to mimic the pattern on the opposite substrate. The process flow is also slightly different from the previous case. Here, only the transmissive substrate is coated with the photo-alignment layer and exposed to the interference pattern. Then the sandwich of the two substrates is made and the LC is filled.

To provide the degenerate alignment condition, after cleaning our mirrors we spin-coat 3-GPS at 5000 RPM for 30 s and then cure the layer at 170 C for 1 hour. The other substrate is processed the same way as before. The LC filling conditions are also the same. An important distinction has to be made at this point. The 3-GPS layer by itself cannot create the alignment condition for the LCPG, due to its degenerate-planar character, and leads to an overall lower surface influence on the LC alignment thus decreasing the critical thickness, d_C , as we have pointed this in an earlier work.¹³ Hence for the same LC material, when compared with the previous approach the minimum achievable grating period is larger, which is in agreement with our experimental results that will be discussed in the next section.

5. EXPERIMENTAL RESULTS

Now we present and compare results from samples fabricated using both the above approaches. In the following discussion, the reflectance and the diffraction efficiency of the m^{th} diffracted order are defined as:

$$R_m = I_m / I_{in}, \quad (4)$$

$$\eta_m = I_m / \Sigma I_m \quad (5)$$

where I_m is the intensity measured in that order and I_{in} is the intensity of input light. It is important to note that while both the efficiency η_m and the reflectance R_m include the inherent diffraction efficiency (from the grating itself), only the latter includes the aggregate effect of all other potential losses: air-glass Fresnel losses, substrate/electrode loss, mirror loss, and any scattering loss. The data presented here is for the following two representative samples, with Sample A fabricated using the UV absorber and Sample B using 3-GPS respectively:

1. SAMPLE A: $\Lambda = 2.2\mu\text{m}$, $d = 1.4\mu\text{m}$, liquid crystal MDA-06-177 (MERCK, $\Delta n = 0.1434$, $T_{NI} = 100.5^\circ\text{C}$, $K_1 = 15.3\text{pN}$, $K_3 = 16.1\text{pN}$, $\Delta\epsilon = 6.1$, $\gamma_1 = 106\text{mPa-s}$)
2. SAMPLE B: $\Lambda = 4.9\mu\text{m}$, $d = 1.5\mu\text{m}$, liquid crystal MLC-12100-000 (MERCK, $\Delta n = 0.113$, $T_{NI} = 92^\circ\text{C}$, $K_1 = 11.4\text{pN}$, $K_3 = 13.8\text{pN}$, $\Delta\epsilon = 8.5$, $\gamma_1 = 183\text{mPa-s}$)

5.1. Reflectance and Contrast Ratio

Fig. 4(a) compares the reflectance vs. voltage curve for the 0-order R_0 and the sum of the first orders $\Sigma R_{\pm 1}$ for both these samples measured with a He-Ne laser (633 nm). Highly-efficient diffraction with very low scattering can be observed. As the voltage is increased, Freedericksz transition is observed at a threshold voltage of $V_{th} \approx 1.8V$ for Sample A while for Sample B, it is at 1.0 V. At higher voltages, the LC molecules reorient themselves along the applied field which erases the grating operation. This couples most of the light into the 0-order as observed in the plot and incoherent scattering (light reflected anywhere except the diffraction orders) was observed less than 3%. Reflectances are almost as high as 90% can be noted for both the samples. The dotted line represents the measured reflectance from a blank cell made with an ITO substrate and an aluminum

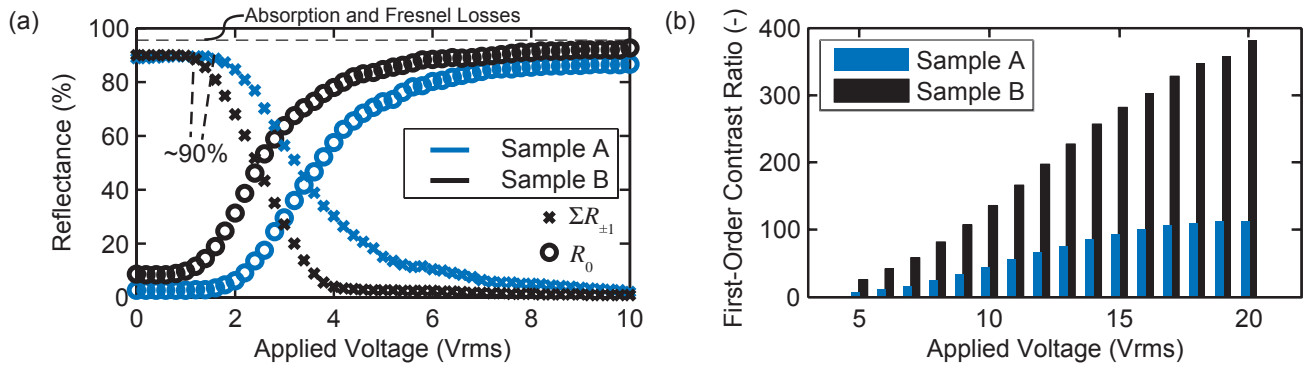


Figure 4. (a) Reflectances of the sum of first orders $\Sigma R_{\pm 1}$ and the 0-order R_0 as a function of applied RMS voltage for Sample A and B respectively. Circles correspond to the 0-order while crosses correspond to the sum of the first orders. (b) Sum of first order contrast ratios for both the samples measured at different voltages for an incident angle of 5° . A vertically polarized He-Ne laser ($\lambda = 633\text{nm}$) was used for measurement.

mirror (filled with glue), that accounts for any absorption or Fresnel losses. As a result, the maximum inherent first-order diffraction efficiency was 95% for both Sample A and B, if we normalize out the substrate losses. The sum of the first order (electrical) contrast ratio for both samples is shown in Fig. 4(b). The contrast ratio for the sum of the first orders is defined as $CR = \max(\Sigma I_{\pm 1}) / \Sigma I_{\pm 1}$ where $\Sigma I_{\pm 1}$ is the sum of the measured intensities in both the first orders. Here we see a marked difference between the two approaches. The values for Sample B ($\sim 400:1$ at 22V) are a lot higher than for Sample A ($\sim 100:1$ at 22V). We attribute this to the degenerate planar anchoring of 3-GPS, as opposed to the strong anchoring condition of the photo-alignment layer, that causes the LC molecules to align more easily at the surface in the direction of the electric field. We should mention that even though Samples A and B present the best overall results from these methods, we have been able to get similar (but not consistent or uniform) results using these approaches down to grating periods of $1.9\mu\text{m}$ and $3.5\mu\text{m}$, respectively.

5.2. Polarization Sensitivity

The polarization sensitivity of these reflective samples was also measured by using the He-Ne laser. We only present data for Sample A, the data for Sample B is similar. Fig. 5(a) and Fig. 5(b) shows the variation of diffraction efficiency as the linearly polarized light from the laser is passed through a QWP, whose optical axis is rotated. This corresponds to a change in the polarization state of the light incident on the LCPG. From Eq. (2), this corresponds to modulating S'_3 between -1 and 1. If we consider a reflective LCPG with $d \approx \lambda / (4\Delta n)$, then according to Eq. (2) this change in S'_3 should modulate the individual first order efficiencies between 0 to a 100%. In both Fig. 5(a) and (b), we can see that a similar variation can be observed in both the first orders, with the diffraction efficiencies varying from $\approx 0\%$ to $\approx 95\%$.

This polarization sensitivity of the first orders can be quantified by a polarization contrast defined as $\max(\eta_m) / \min(\eta_m)$. From the measured data in Fig. 5(a) and (b), these extremum points occur when the incident light is circularly polarized i.e. when the fast axis of the QWP is at $45^\circ, 135^\circ, 225^\circ$ or 315° . A high polarization contrast generally indicates that a good quality hologram has been created. Polarization contrast in the first orders was measured to be as high as $>2000:1$ for Sample A and $>4000:1$ for Sample B. Even though the diffraction efficiencies of individual first-orders are highly polarization sensitive, their sum remains polarization independent as Eq. (2) shows. This fact, and the natural polarization insensitivity (absence of S'_3 in Eq. (1)) of the 0-order enables polarization independent modulation. On the other hand, the rotation of a Half Waveplate (HWP) should not theoretically cause a change in the diffraction efficiencies of the first orders since the polarization simply undergoes a rotation. This can also be roughly verified from the data in Fig. 5(c) and Fig. 5(d).

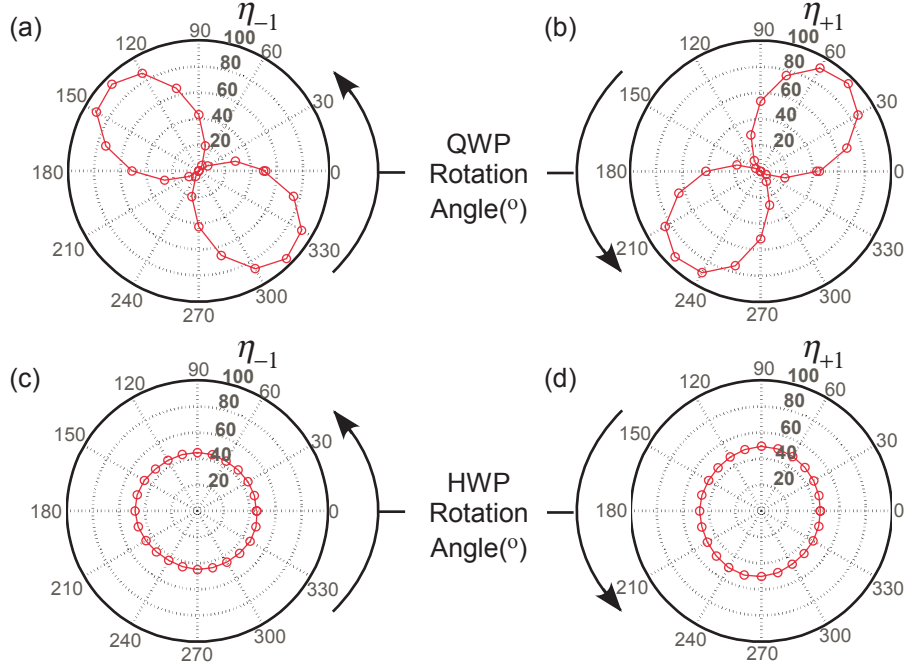


Figure 5. Measured diffraction efficiencies on Sample A of the (a) -1 order and (b) +1 order in response to rotation of a quarter waveplate. Measured diffraction efficiencies of the (c) -1 order and (d) +1 order in response to rotation of a half waveplate. Angle of incidence was fixed at 5° and a He-Ne laser ($\lambda = 633\text{nm}$) was used for the measurements.

5.3. Dynamic Response

As mentioned before, the dynamic response for these structures is expected to be much faster than the transmissive mode. Fig. 6 shows the rise time t_{on} and the fall time t_{off} as a function of the applied voltage, for both Sample A and Sample B. From our earlier work,¹³ analytic expressions for the rise and fall times, neglecting LC flow effects, are given by:

$$t_{on} = \frac{\ln(9)\gamma_1^* d^2}{\epsilon_0 \Delta\epsilon (V^2 - V_{th}^2)}, \quad (6)$$

$$t_{off} = \frac{\ln(9)\gamma_1^* d^2}{\epsilon_0 \Delta\epsilon V_{th}^2}. \quad (7)$$

Here V is the applied voltage and V_{th} is the threshold voltage that assumes the following form:

$$V_{th} = \pi \sqrt{\frac{K_1}{\epsilon_0 \Delta\epsilon}} \sqrt{1 - \left(\frac{d}{d_C}\right)^2}. \quad (8)$$

In these expressions, γ_1^* is an effective viscosity parameter¹⁷ that depends strongly on the rotational viscosity, γ_1 and is generally introduced to approximately account for any LC flow effects on the dynamic response. Although information about specific material properties such as the Leslie viscosities¹⁷ is needed to correlate these analytic expressions to actual measurements, we note that $\gamma_1^*/\gamma_1 \approx 0.2, 0.125$ for Samples A and B respectively, provides a good fit to our data shown in Fig. 6. For both Sample A and Sample B, as voltage is increased, t_{on} decreases sharply, while on the other hand t_{off} stays constant, which is also predicted by Eqs. (6) and (7). The difference in magnitude of switching times between the two samples is because of the parameters indicated ($\Delta\epsilon$ is almost the same). But notice that for Sample A, at a voltage of $10V$, $t_{on} \approx 100\mu\text{s}$ and $t_{off} \approx 500\mu\text{s}$, which are much faster than most LC modes used commercially.¹⁸

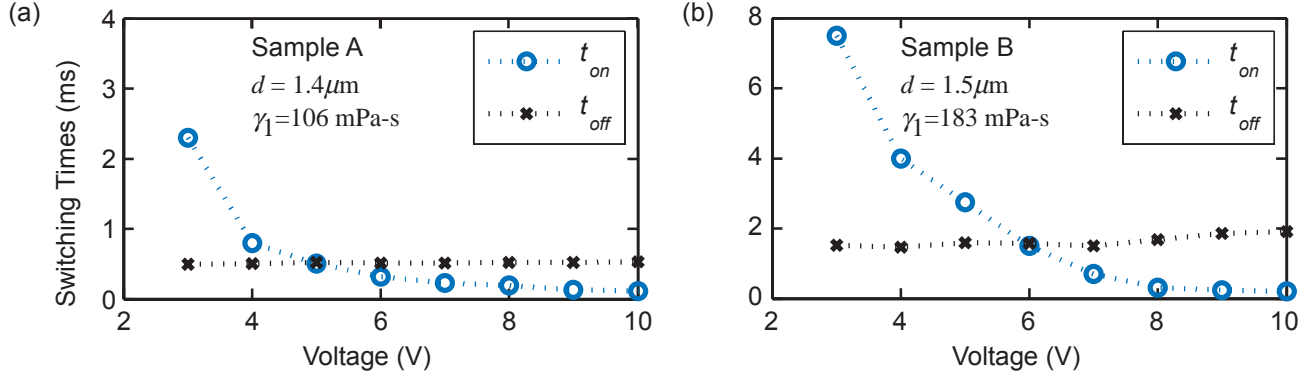


Figure 6. Electrical rise t_{on} and fall t_{off} times measured at different voltages for (a) Sample A, and (b) Sample B respectively.

5.4. Effects of Oblique Incidence

The expressions in Eqs. (1) and (2) are sufficient to analyze reflective LCPGs for small incident angles, typically $\leq 5^\circ$. Although techniques such as the Extended Jones Matrix method¹⁹ can be used to derive analytical expressions for off-axis incidence, a paraxial approximation is generally used that limits their scope. Numerical methods such as the Finite-Difference-Time-Domain (FDTD)^{20, 21} approach are the preferred means to analyze oblique incidence effects.

Fig. 7 shows the measured diffraction efficiencies for Sample A at different incident angles, along-with simulated results from WOLFSIM,²⁰ a numerical tool developed based on the FDTD method, for the same essential parameters. Even for large incident angles $\leq 20^\circ$, more than 80% of the light is diffracted into the first orders. However for larger incident angles, the light from the first orders tend to couple into, and thus increase the leakage in the 0-order. From the data in Fig. 7, as θ_{in} increases beyond 45° , more than 50% of the light leaks into the 0-order. Even though an ideal mirror was assumed for simulations, good correspondence can be noted between FDTD predictions and the actual measurement.

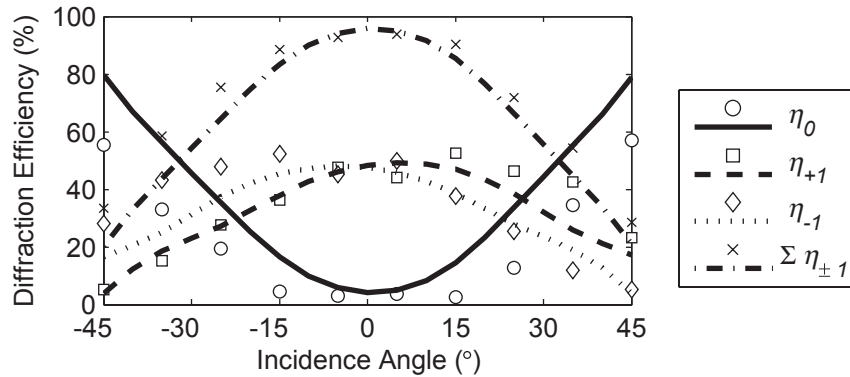


Figure 7. Angular sensitivity of the diffraction behavior of Sample A. The discrete points correspond to experimental data, while the curves correspond to numerical simulation results calculated using the FDTD method.²⁰

6. CONCLUSIONS

In conclusion, we have successfully demonstrated high efficiency reflective LCPGs on aluminum mirrors for the first time. Nearly ideal properties are observed, with diffraction efficiencies approaching 95% and contrast ratios exceeding 400:1 at applied voltages up to 22 V. Reflective mode implementation has also resulted in fast switching LCPGs that can now be modulated with electrical response times as low as $600 \mu\text{s}$, and has favored fabrication at

small grating periods as low as $2.2\mu\text{m}$, resulting in much larger diffraction angles than before. These significant improvements indicate that reflective LCPGs are excellent candidates for both polarization independent and polarization sensitive modulation. The ideas and fabrication processes presented here are generally applicable to any reflective substrate, and thus can be easily extended to LCOS technology. Hence highly-efficient reflective SLMs based on LCPGs present a wide variety of opportunities in applications such as telecommunication light control elements, beam-steering, displays and spatial-light-modulators.

ACKNOWLEDGMENTS

We gratefully acknowledge support from National Science Foundation (ECCS-0621906) and the Kenan Institute for Engineering, Technology, and Science.

REFERENCES

1. J. Tervo and J. Turunen, "Paraxial-domain diffractive elements with 100% efficiency based on polarization gratings," *Optics Letters* **25**(11), pp. 785–786, 2000.
2. J. N. Eakin, Y. Xie, R. A. Pelcovits, M. D. Radcliffe, and G. P. Crawford, "Zero voltage freedericksz transition in periodically aligned liquid crystals," *Applied Physics Letters* **85**(10), pp. 1671–1673, 2004.
3. M. J. Escuti and W. M. Jones, "Polarization independent switching with high contrast from a liquid crystal polarization grating," *SID Symposium Digest* **37**, pp. 1443–1446, 2006.
4. R. K. Komanduri, W. M. Jones, C. Oh, and M. J. Escuti, "Polarization-independent modulation for projection displays using small-period LC polarization gratings," *Journal of the Society for Information Display* **15**(8), pp. 589–594, 2007.
5. T. J. Bunning, L. V. Natarajan, V. P. Tondiglia, and R. L. Sutherland, "Holographic polymer-dispersed liquid crystals (H-PDLCs)," *Annual Review of Materials Science* **30**, pp. 83–115, 2000.
6. J. Chen, P. J. Bos, H. Vithana, and D. L. Johnson, "An electrooptically controlled liquid-crystal diffraction grating," *Applied Physics Letters* **67**(18), pp. 2588–2590, 1995.
7. C. M. Titus and P. J. Bos, "Efficient, polarization-independent, reflective liquid crystal phase grating," *Applied Physics Letters* **71**(16), pp. 2239–2241, 1997.
8. C. C. Bowley and G. P. Crawford, "Improved reflective displays based on polymer-dispersed liquid crystals," *Journal of Optical Technology* **67**(8), pp. 717–722, 2000.
9. M. Honma and T. Nose, "Liquid-crystal reflective beam deflector with microscale alignment pattern," *Japanese Journal of Applied Physics Part 1* **43**(12), pp. 8151–8155, 2004.
10. V. K. S. Hsiao, T. C. Lin, G. S. He, A. N. Cartwright, P. N. Prasad, L. V. Natarajan, V. P. Tondiglia, and T. J. Bunning, "Optical microfabrication of highly reflective volume bragg gratings," *Applied Physics Letters* **86**(13), 131113, 2005.
11. F. Gori, "Measuring stokes parameters by means of a polarization grating," *Optics Letters* **24**(9), pp. 584–586, 1999.
12. M. Schadt, H. Seiberle, and A. Schuster, "Optical patterning of multidomain liquid-crystal displays with wide viewing angles," *Nature* **381**(6579), pp. 212–215, 1996.
13. R. K. Komanduri and M. J. Escuti, "Elastic continuum analysis of the liquid crystal polarization grating," *Physical Review E* **76**(2), 021701, 2007.
14. E. Hecht, *Optics*, Addison and Wesley, New York, 1998.
15. M. Zayat, P. Garcia-Parejo, and D. Levy, "Preventing uv-light damage of light sensitive materials using a highly protective uv-absorbing coating," *Chemical Society Reviews* **36**(8), pp. 1270–1281, 2007.
16. I. Dozov, D. N. Stoenescu, S. Lamarque-Forget, P. Martinot-Lagarde, and E. Polossat, "Planar degenerated anchoring of liquid crystals obtained by surface memory passivation," *Applied Physics Letters* **77**(25), pp. 4124–4126, 2000.
17. I. W. Stewart, *The static and dynamic continuum theory of liquid crystals : a mathematical introduction*, Taylor and Francis, London ; New York, N.Y., 2004.
18. K. Takatoh, M. Hasegawa, M. Koden, N. Itoh, R. Hasegawa, and M. Sakamoto, *Alignment Technologies And Applications Of Liquid Crystal Devices*, Taylor and Francis, New York, 2005.

19. P. Yeh and C. Gu, *Optics of Liquid Crystal Displays*, Wiley, New York, 1999.
20. C. Oh and M. J. Escuti, "Numerical analysis of polarization gratings using the finite-difference time-domain method," *Physical Review A* **76**(4), 043815, 2007.
21. C. Oh and M. J. Escuti, "Time-domain analysis of periodic anisotropic media at oblique incidence: an efficient FDTD implementation," *Optics Express* **14**(24), pp. 11870–11884, 2006.